第 34 卷第 3 期
2015 年 6 月

红 外 与 毫 米 波 学 报
J. Infrared Millim. Waves

Vol. 34, No. 3
June, 2015

文章编号: 1001 - 9014(2015)03 - 0276 - 06

DOI:10.11972/j.issn.1001 - 9014.2015.03.004

Two-wavelength IR signals based on optical frequency mixing

SHI Gang[1*], ZHU Chang-Jun[2], XUE Bing[2], ZHAI Xue-Jun[2]

(1. School of Science, Chang'an University, Xi'an 710064, China;
2. School of Science, Xi'an Polytechnic University, Xi'an 710048, China)

Abstract: Optical signals of two different wavelengths in the IR regime were generated in atomic Rb vapor using broad bandwidth laser pulses. Competition between the two signals was observed. The effects of pump laser intensity, chirp of laser pulses and Rb number density on the characteristics of the two signals were investigated. The results show that the two signals were generated from two coupled parametric six-wave mixings processes and the competition between the two signals was dominantly governed by phase matching conditions related to Rb number density.

Key words: six-wave mixings, coupled channels, IR signals, phase matching
PACS: 42.65.-K, 42.65.Lm, 42.65.Ky

基于光学混频的双波长红外信号

石 刚[1*], 朱长军[2], 薛 兵[2], 翟学军[2]
(1. 长安大学 理学院,陕西 西安 710064;
2. 西安工程大学 理学院,陕西 西安 710048)

摘要:采用宽带宽的光脉冲在铷原子蒸汽中产生两个红外波段双波长的光信号,观察到两个红外光信号间存在竞争。研究了泵浦激光强度、光脉冲啁啾和铷原子数密度对两个红外光信号特性的影响。结果表明,两个红外光信号产生于两个耦合的参量六波混频过程;信号的强度随泵浦激光强度、光脉冲啁啾和铷原子数密度发生变化,两个波长红外光信号间的竞争主要由与铷原子数密度相关的相位匹配条件所决定。

关 键 词:红外信号;六波混频;耦合通道;相位匹配

中图分类号:O657.33 **文献标识码**:A

Introduction

Nonlinear optical wave mixing is widely employed to achieve optical frequency conversion in a wide wavelength range. So far, much attention has been focused on this issue. In particular, optical four-wave mixing (FWM) and six-wave mixing (SWM) in gas medium have attracted considerable attention due to the controllable refractive indices of the gas media. To date, intensive researches have been conducted on FWM and SWM in many alkali atomic vapors, such as sodium [1], potassium[2], lithium [3] and mixed sodium-potassium[4]. Ultrashort light pulses have been converted efficiently to the infrared range of the frequency[5]. Moreover, competition between two FWM channels via atomic coherence has been studied in Rb[6], and the interplay between FWM and SWM processes has been observed in Rb via dual electromagnetically induced transparency windows[7]. Recently, conversion between enhancement and suppression in SWM and fluorescence signals has been demonstrated by phase modulation[8]. Furthermore, nonreciprocity of six-wave mixing has been controlled by a moving electromagnetically induced grating[9].

Little attempt, however, has hitherto been dedicated to studying the generation and control of the coupled two-wavelength or multi-wavelength signals using optical wave mixing [10]. Generation and control of optical signals in a wide wavelength range is of significant importance in optical gates and coherent control. A compre-

Received date: 2014 - 09 - 03, **revised date**: 2014 - 10 - 22 **收稿日期**:2014 - 09 - 03, **修回日期**:2014 - 10 - 22
Foundation items: Supported by the Program for the National Natural Science Foundation of China (51101022), Key Science and Technology Program of Shaanxi Province of China (2013K06-27)
Biography: SHI Gang(1972-), male, Xian, chang'an university, associate Professor, PHD, research on nonlinear optics, optoelectronics and laser spectroscopy
* **Corresponding author**: E-mail: shigang_xa@126.com

hensive study on the interplay between optical signals not only unravels the underpinning mechanisms for the mutual interplay of the related processes, but also has potential applications in producing multi-channel ultrafast optical gates. We present in this paper a study on the mutual interplay between two coupled SWM channels in Rb vapour, in which two-wavelength signals are generated.

1 Theory on FWM and SWM

We consider a four-wave mixing process involving merely one idler. In this situation, the pump electric field induces polarization at the signal and idler frequencies and, then, generates emissions at the signal and idler frequencies. Using the slowly varying envelope assumption for the radiation, which is valid for the ~120-fs pulses, the total electric field can be expressed as

$$E(z,t) = \frac{1}{2}\left[A_p(z)e^{-j(\omega_p t-k_p z)} + A_i(z)e^{-j(\omega_i t-k_i z)} + A_s(z)e^{-j(\omega_s t-k_s z)} + c.c.\right] \quad , \quad (1)$$

where A's represent complex field amplitudes, and $c.c.$ stands for complex conjugate. Under the quasistatic approximation, the amplitudes of the individual fields in Eq. (1) obey a system of coupled wave equations that, for collinear plane waves, is expressed as

$$2jk_x\frac{\mathrm{d}A_x}{\mathrm{d}z} = -\frac{4\pi\omega_x^2}{c^2}P^{(3)}(\omega_x)e^{-j\Delta kz} \quad , \quad (2)$$

where $x = p, i, s$, respectively, $\Delta k = 2\omega_p n_p - \omega_i n_i - \omega_s n_s$ is the wavevector mismatch, $P^{(3)}(\omega_{p,i,s})$ represents the third-order nonlinear polarization amplitudes induced by the electric field at the pump, idler and signal frequencies, respectively, given by

$$\begin{aligned} P^{(3)}(\omega_p) &= \frac{3}{2}\chi^{(3)}(-\omega_p,\omega_s,-\omega_p,\omega_i)A_sA_p^*A_i \\ P^{(3)}(\omega_i) &= \frac{3}{4}\chi^{(3)}(-\omega_i,-\omega_s,\omega_p,\omega_p)A_s^*A_p^2 \\ P^{(3)}(\omega_s) &= \frac{3}{4}\chi^{(3)}(-\omega_s,\omega_p,\omega_p,-\omega_i)A_p^2A_i^* \end{aligned} \quad . (3)$$

Then, the intensity of the output four-wave mixing signal is determined by

$$I_s \propto |P^{(3)}(\omega_s)|^2 \propto |\chi^{(3)}A_p^2A_i^*|^2 \quad , \quad (4)$$

For six-wave mixing, similar procedure can be applied, and we obtain

$$\begin{aligned} P^{(5)}(\omega_p) &\propto \chi^{(5)}(-\omega_p,\omega_s,-\omega_p,\omega_{i1},\omega_{i2},\omega_{i3})A_sA_p^*A_{i1}A_{i2}^*A_{i3}^* \\ P^{(5)}(\omega_{i1}) &\propto \chi^{(5)}(-\omega_{i1},-\omega_s,\omega_p,\omega_p-\omega_{i2},-\omega_{i3})A_s^*A_p^2A_{i2}^*A_{i3}^* \\ P^{(5)}(\omega_{i2}) &\propto \chi^{(5)}(-\omega_{i2},-\omega_s,\omega_p,\omega_p-\omega_{i1},-\omega_{i3})A_s^*A_p^2A_{i1}^*A_{i3}^* \\ P^{(5)}(\omega_{i3}) &\propto \chi^{(5)}(-\omega_{i3},-\omega_s,\omega_p,\omega_p-\omega_{i2},-\omega_{i1})A_s^*A_p^2A_{i2}^*A_{i1}^* \\ P^{(5)}(\omega_s) &\propto \chi^{(5)}(-\omega_s,\omega_p,\omega_p,-\omega_{i1},-\omega_{i2},-\omega_{i3})A_p^2A_{i1}^*A_{i2}^*A_{i3}^* \end{aligned} \quad . (5)$$

Then, the intensity of the output six-wave mixing signal is given by

$$I_s \propto |P^{(5)}(\omega_s)|^2 \propto |\chi^{(5)}A_p^2A_{i1}^*A_{i2}^*A_{i3}^*|^2 \quad . (6)$$

2 Experimental setup

Fig. 1(a) shows partial Rb energy levels involving in difference-frequency FWM, $5^2S_{1/2}\rightarrow\rightarrow7^2S_{1/2}\rightarrow6^2P_{3/2}\rightarrow5^2S_{1/2}$, in which $7^2S_{1/2}$ state is excited by two-photon transition. Emissions at 3 969 nm (near $7^2S_{1/2}\rightarrow6^2P_{3/2}$ transition) and 420 nm (near $6^2P_{3/2}\rightarrow5^2S_{1/2}$ transition) can be obtained from the FWM. Simultaneously, difference-frequency SWM can occur together with the FWM as the $7^2S_{1/2}$ state is excited two-photon transition. Fig. 1(b) shows partial Rb energy levels involving in difference-frequency SWM, through which resonant transitions $5^2S_{1/2}\rightarrow7^2S_{1/2}$, $7^2S_{1/2}\rightarrow6^2P_{3/2}$, $6^2P_{3/2}\rightarrow6^2S_{1/2}$, $6^2S_{1/2}\rightarrow5^2P_{1/2}$, $6^2S_{1/2}\rightarrow5^2P_{3/2}$, $5^2P_{1/2}\rightarrow5^2S_{1/2}$, $5^2P_{3/2}\rightarrow5^2S_{1/2}$ can occur. The corresponding emissions have wavelengths of 380, 3 970, 2 732, 1 324, 1 366, 795, 780 nm, respectively. On the other hand, difference-frequency SWM may take place by two-photon excitation of $7^2S_{1/2}$ state as laser wavelength is tuned near 760 nm. In this case, the two difference-frequency SWM processes appear in the two coupled channels, $5^2S_{1/2}\rightarrow\rightarrow7^2S_{1/2}\rightarrow6^2P_{3/2}\rightarrow6^2S_{1/2}\rightarrow5^2P_{1/2}\rightarrow5^2S_{1/2}$ and $5^2S_{1/2}\rightarrow\rightarrow7^2S_{1/2}\rightarrow6^2P_{3/2}\rightarrow6^2S_{1/2}\rightarrow5^2P_{3/2}\rightarrow5^2S_{1/2}$, respectively, since $6^2S_{1/2}$ is shared by the two channels in the SWM processes.

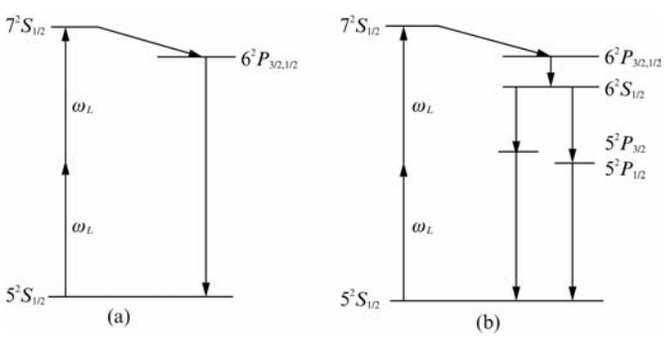

Fig. 1　Rb energy levels involved in the (a) FWM and (b) two coupled SWM processes

图 1　Rb 原子中(a)四波混频和(b)两个耦合的六波混频过程涉及的能级

Experimental setup shown in Fig. 2 was used to investigate FWM and SWM in Rb. A 1-kH Ti:sapphire laser amplifier system generated laser pulses with energy of 1 mJ and 120 fs pulse duration. The wavelength of laser pulse was tunable and centered at 760 nm in order to excite the $7^2S_{1/2}$ state of Rb by two-photon excitation. Laser pulses from the amplifier were attenuated and then focused by a 25-cm-focal-length lens into a sapphire cell containing Rb, in which the number density of Rb atoms

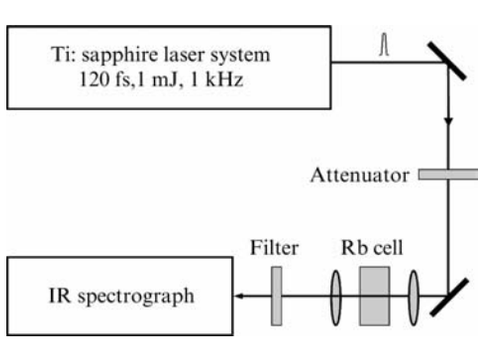

Fig. 2　Schematic diagram of the experimental arrangement

图 2　实验装置示意图

was adjustable by employing a heating oven. Collinearly propagating emissions from the cell were filtered by IR filters and, then, detected by visible and infrared optical spectrographs.

3 Results and discussions

Experiments were first conducted at pump laser intensity of 2×10^{10} Wcm^{-2}, Rb number density of $2 \times 10^{16} cm^{-3}$ and the laser pulse was chirp free. Coherent emissions at 420 nm, 781 nm and 793 nm were generated in the visible regime, as shown in Fig. 3(a). Concurrently, coherent emissions at 1 323 nm, 1 367 nm, 2 731 nm and 3 969 nm were generated in the IR regime, as shown in Fig. 3(b). Note that the spectrum of the residue of pump laser is centered at 760 nm. Inspection of Fig. 1(a) and Fig. 3(b) indicates that emissions at 420 nm and 3 969 nm are generated by FWM and, on the other hand, emissions at 781 nm, 793 nm, 1 323 nm, 1 367 nm, 2 731 nm and 3 969 nm are produced by two SWM processes. As an infrared filter was implemented to block the residue of the laser, emission at 420 nm, which stems from the FWM, is much strong as compared with the residue of laser, around 760 nm. Emission at 3 969 nm is generated by both FWM and SWM and, hence, is much stronger than other emissions produced by SWM. The mechanism for strong signal and idler in the FWM compared with that in the SWM lies in that the third order susceptibility $\chi^{(3)}$ related to FWM is several orders of magnitude larger than the fifth order susceptibility $\chi^{(5)}$ associated with SWM.

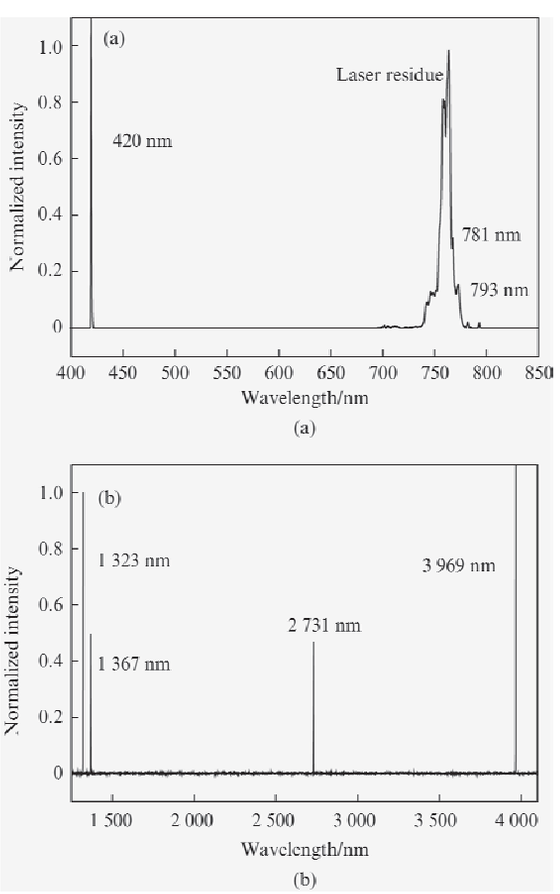

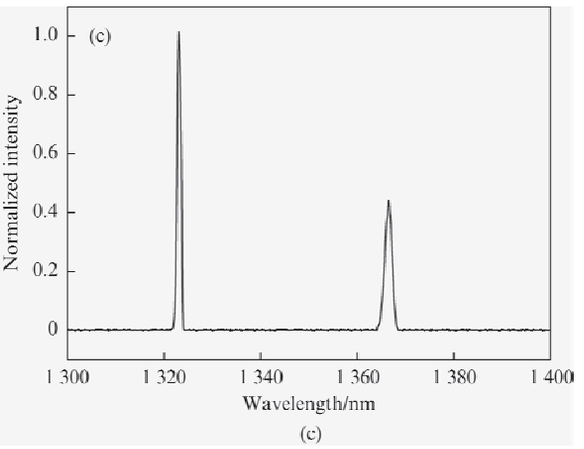

Fig. 3 Coherent emissions in the (a) visible, (b) IR region and (c) SWM signals at 1 323 nm and 1 367 nm at pump laser intensity 2×10^{10} W cm^{-2} and Rb number density $2 \times 10^{16} cm^{-3}$

图3 相干辐射信号(a)可见光范围,(b)红外光谱范围,(c)波长为1 323 nm和1 367 nm的六波混频信号,泵浦激光强度 2×10^{10} W cm^{-2},Rb原子数密度 $2 \times 10^{16} cm^{-3}$

As emissions at 1 323 nm and 1 367 nm display interplay as experimental parameters are changed, we designate the two emissions as signals and focus attention on the interplay. Signals at 1 323 nm and 1 367 nm on expanded scale are shown in Fig. 3(c). Interestingly, signals at 1 323 nm and 1 367 nm are in close proximity to the $6^2S_{1/2} \rightarrow 5^2P_{1/2}$ and $6^2S_{1/2} \rightarrow 5^2P_{3/2}$ transitions. The resonant transition wavelengths for $6^2S_{1/2} \rightarrow 5^2P_{1/2}$ and $6^2S_{1/2} \rightarrow 5^2P_{3/2}$ are 1 324 nm and 1 366 nm, respectively. In contrast, the central wavelengths of IR signals are not equal to the corresponding resonant transition wavelengths, suggesting that the signals are not originated from resonant emission. Moreover, the coherent emissions were only observed in the forward direction in the experiments. The competition between FWM and ASE was analyzed theoretically and, in the meantime, the survival of FWM and suppression of ASE were demonstrated experimentally [11]. On the other hand, the spectral width of the signals at 1 323 nm and 1 367 nm are 1 ~ 2 nm, much broader than the spectral width of resonant transitions, indicating that SWM occurs at different signal wavelengths because of the broad bandwidth of the pump laser pulses. Therefore, the experimentally observed signals are predominantly produced from parametric SWM processes, which are quite similar to parametric FWM in several respects. One of them is that the competition between parametric FWM and amplified spontaneous emission causes the suppression of the latter[11]. The two parametric SWM channels share the same energy level in Rb, $6^2S_{1/2}$, causing a coupling and, hence, a signal competition between the two channels. The interplay between the two signals is associated with several parameters, the influences of which are examined in the following subsections.

3.1 Influence of laser intensity on the signals

To investigate the influences of pump laser intensity on the interplay of the parametric SWM signals, experiments were furthermore performed with various pump laser intensities, ranging from 1.8×10^9 Wcm^{-2} to $7 \times$

10^{12} Wcm^{-2}. The Rb number density was 2×10^{16} cm^{-3} and the laser pulse was chirp free. The results are shown in Fig. 4. It can be seen that both the signals increase with the pump laser intensity. Specifically, the increasing rate of the signal is large as the pump laser intensity is below 3×10^{11} Wcm^{-2}, the increasing rate of the signal becomes small as the pump laser intensity is above 3×10^{11} Wcm^{-2}. This feature might be attributed to the following mechanisms. First, the ionization rate of Rb atoms increases as the pump laser intensity increases, leading to a decreasing effective Rb number density and, hence, a decreasing signal. Second, the ionization of Rb atoms causes defocusing effect of the pump laser beam at the focal point, resulting in a decrease of effective pump laser intensity and, hence, a saturation of the signals. In collinear case, phase mismatch in a parametric SWM process is defined as

$$\Delta k = \frac{1}{c}\left[2n(\omega_1)\omega_1 - n(\omega_2)\omega_2 - n(\omega_3)\omega_3 - n(\omega_4)\omega_4 - n(\omega_5)\omega_5\right], \quad (7)$$

where c is the light speed in vacuum, $n(\omega)$ is the refractive index of the medium, ω_1 is the angular frequency of the pump light, ω_2 is the angular frequency of the signal, ω_3, ω_4 and ω_5 are the angular frequencies of the idlers. The refractive index $n(\omega)$ can be expressed in the form

$$n(\omega) = n_0(\omega) + n_2(\omega)I, \quad (8)$$

where $n_0(\omega)$ is the linear refractive index of the medium, $n_2(\omega)I$ is the nonlinear refractive index induced by the Kerr effect, I is the pump laser intensity. The nonlinear refractive index induced by the Kerr effect is quite small in gas medium compared with that in solid and liquid medium. Consequently, the difference of the nonlinear refractive indices for the two wavelengths of the IR signals is extremely small, leading to a result that the phase matching condition remains nearly unchanged. Thus, both the signals increase with the pump laser intensity at approximately equal rate. In other words, pump laser intensity exerts little influences on the interplay of the parametric SWM signals.

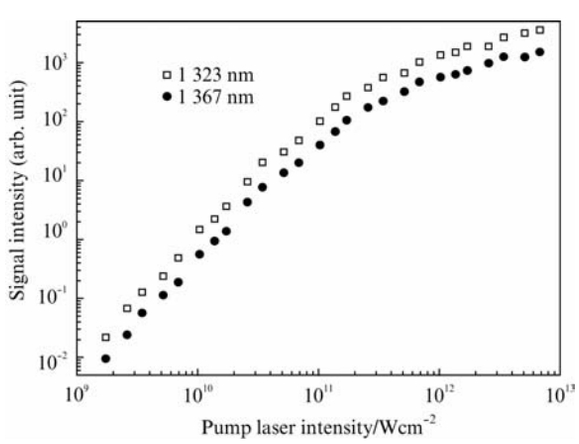

Fig. 4　Variation of parametric SWM signals with pump laser intensity at Rb number density 2×10^{16} cm^{-3}

图 4　参量六波混频信号强度随泵浦激光强度的变化，Rb 原子数密度 2×10^{16} cm^{-3}

3.2　Influence of pump pulse chirp on the signals

Experiments were conducted with different chirp parameters of the laser pulses, with pump laser pulse energy fixed at 1 μJ (corresponding to an intensity of 2×10^{10} Wcm^{-2} at the focus for chirp free pulses), Rb number density of 2×10^{16} cm^{-3}. Fig. 5 shows the experimental results. It can be seen that both the parametric SWM signals reach maxima as the pump laser pulse is free of chirp. As the chirp parameter increases, the parametric SWM signals decreases and, moreover, positive and negative chirps contribute equally to the decrease of the parametric SWM signals. This feature might be attributed to the following mechanism. As the laser pulse is chirped, the width of the laser pulse increase since the laser pulse energy is fixed. The positive and negative chirp parameters lead to the broadening of laser pulses equally. Consequently, the peak intensity of the laser pulse decrease with increasing chirp parameter and, hence, the parametric SWM signals, which are closely related to the pump laser intensity, decrease monotonically.

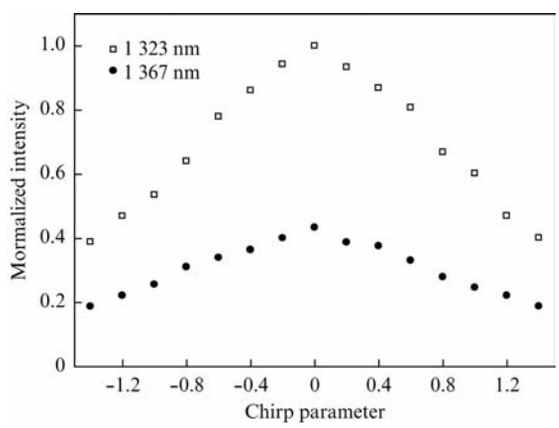

Fig. 5　Variation of parametric SWM signals with chirp parameter of the pump laser pulses at pump laser pulse energy 1 μJ and Rb number density 2×10^{16} cm^{-3}

图 5　参量六波混频信号强度随泵浦激光啁啾参量的变化，泵浦激光脉冲能量 1 μJ，Rb 原子数密度 2×10^{16} cm^{-3}

3.3　Influence of Rb number density on the signals

To gain an insight into the influences of Rb number density on the interplay of the parametric SWM signals, experiments were furthermore performed with various Rb number densities, ranging from 0.5×10^{16} cm^{-3} to 5×10^{16} cm^{-3}. The pump laser intensity was fixed at 2×10^{10} Wcm^{-2} and the laser pulse was chirp free. Fig. 6 shows the experimental results. It can be seen that both the parametric SWM signals vary with Rb number density. Specifically, The signal at 1 323 nm increases with Rb number density and reaches a maximum value as the Rb number density is around 2.6×10^{16} cm^{-3} and, then, decreases with Rb number density. Similarly, the signal at 1 367 nm increases with Rb number density and reaches a maximum value as Rb number density is around 1.3×10^{16} cm^{-3} and, then, decreases with Rb number density. As the Rb number density ranges from 1.7×10^{16} cm^{-3} to 2.6×10^{16} cm^{-3}, the two signals exhibit a competition, i. e., the signal at 1 323 nm increases whereas the signal at 1 367 nm decreases.

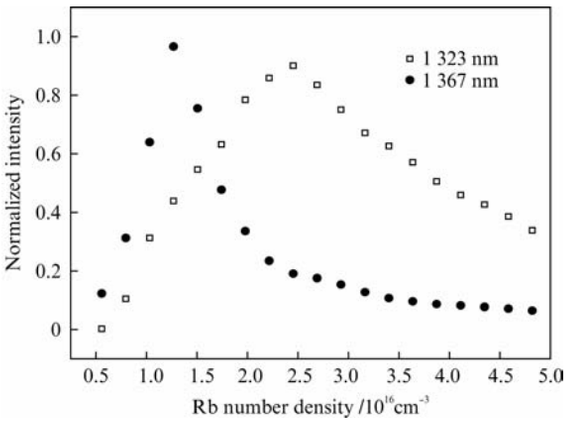

Fig. 6 Variation of parametric SWM signals with Rb number density at pump laser intensity 2×10^{10} W cm^{-2}

图6 参量六波混频信号强度随Rb原子数密度的变化,泵浦激光强度 2×10^{10} W cm^{-2}

Further insight into the competition occurring in these experiments is provided by investigating phase matching conditions for each parametric SWM process. The refractive index $n(\omega)$ is expressed as[12]

$$n(\omega)^2 = 1 + \frac{2\pi Ne^2}{m_e}\sum_i \frac{f_{ig}}{(\omega_{ig}^2 - \omega^2)}, \quad (9)$$

where N is the atomic number density, e and m_e are the charge and the mass of the electron, f_{ig} and ω_{ig} are the oscillator strength and the transition frequency between the excited state i and ground state g of the atom. The values of the oscillator strengths and the transition frequencies in Rb were taken from Ref. [13] and, subsequently, the refractive indices of the Rb near the wavelengths of the pump light, signals and idlers were calculated at different Rb number densities. For a given Rb number density, phase mismatches in one parametric SWM channel were calculated by substituting wavelengths of pump light, signals and idlers, as well as the corresponding refractive indices, into Eq. (7). For another Rb number density, phase mismatches in the two channels were obtained by repeating the same procedure. Consequently, phase mismatches with Rb number density in two channels were obtained, as shown in Fig. 7.

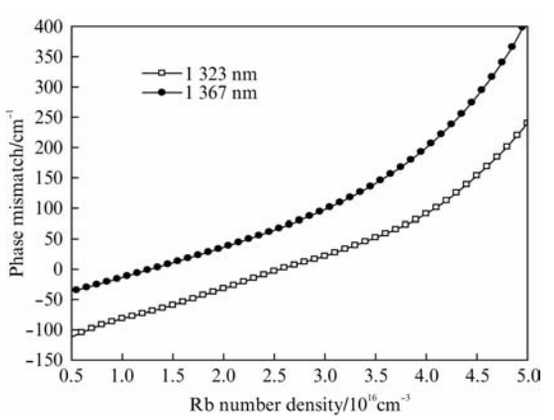

Fig. 7 Phase mismatches in the two parametric SWM channels for different Rb number densities

图7 不同Rb原子数密度下两个参量六波混频通道的相位失配

Comparing the relationship between phase mismatch and signal intensity in the two channels for different Rb number densities unveils further insight into the mechanisms for competition. Close to Rb number density 1.3×10^{16} cm^{-3}, the value of phase mismatch in channel for the signal at 1 323 nm is -71 cm^{-1}, much large compared to the phase mismatch, 2.8 cm^{-1}, in channel for the signal at 1 367 nm (see Fig. 7), resulting in an extremely weaker signal at 1 323 nm than the signal at 1 367 nm, as shown in Fig. 6. However, around Rb number density 2.6×10^{16} cm^{-3}, the value of phase mismatch in channel for the signal at 1 323 nm is 0.6 cm^{-1}, much small compared with the phase mismatch, 69 cm^{-1}, in channel for the signal at 1 367 nm (see Fig. 7), leading to a stronger signal at 1 323 nm than the signal at 1 367 nm, as shown in Fig. 6. Furthermore, from 1.3×10^{16} cm^{-3} to 2.6×10^{16} cm^{-3}, the slopes of the curve in Fig. 6 are much lager than that in Fig. 7, suggesting that the competition between the two channels and, hence, competition between the two signals, is quite sensitive to the phase mismatch. Competition between two FWM channels was investigated previously, in which two FWM signals fall into two simultaneously opened dual electromagnetically induced transparency windows, and the mechanism for the competition was attributed to the mutual dressing effect [6]. Study on coexistence FWM and SWM disclosed competition between FWM and SWM, which is caused by quantum interference effect[7]. The process concerned in current case, however, is parametric process. These effects may appear in the current case, nonetheless, they are not dominant factors governing the competition. Consequently, comparing theoretical calculations with experimental observation provides evidence that phase mismatch varying with Rb number density mainly dominates the competition between the two parametric SWM processes.

4 Conclusions

Two coupled frequency difference six-wave mixings were achieved simultaneously in atomic Rb vapor using laser pulses produced from a Ti:sapphire laser system. Signals at 1 323 nm and 1 367 nm were generated and two coupled six-wave mixing channels were identified. The effects of pump laser intensity, chirp of laser pulses and Rb number density on the characteristics of the signals were analyzed. The results show that signals at 1 323 nm and 1 367 nm primarily stem from parametric SWM process. Moreover, competition between the two signals was observed and phase mismatch determined by Rb number density governs largely the competition between the two parametric SWM processes. Since the competition between the two signals can be controlled by phase mismatch, the applications of the competition in optical gates appear to be promising.

References

[1] Moore M A, Garrett W R, Payne M G. Generation of axially phase-matched parametric four-wave and six-wave mixing in pure sodium vapor[J]. *Phys.* Rev. A 39 (1989): 3692-3695.

[2] Zhang P L, Wang Y C, Schawlow A L. Generation of coherent UV radiation by optical wave-mixing processes in atomic potassium[J]. *J.*

Opt. Soc. Am. B 1 (1984): 9 - 14.

[3] Chen F Z, Han X F, Wu C Y R. High-order stimulated electronic Raman scattering from lithium vapor[J]. *Appl. Phys. B* 56 (1993): 113 -117.

[4] Clark B K, Masters M, Huennekens J. Wave mixing and amplified spontaneous emission in pure potassium and mixed sodium-potassium vapors[J]. *Appl. Phys. B* 47 (1988): 159 - 167.

[5] Sarkisyan D. Efficient converter of the frequency of ultrashort light pulses to the infrared range[J]. *Sov. J. Quantum Electron*. 18 (1988): 1477 - 1479.

[6] Zhang Y P, Anderson B, Brown A W, *et al*. Competition between two four-wave mixing channels via atomic coherence[J]. *Appl. Phys. Lett*. 91 (2007) 061113.

[7] Zhang Y P, Brown A W, Xiao M. Opening Four-Wave Mixing and Six-Wave Mixing Channels via Dual Electromagnetically Induced Transparency Windows[J], *Phys. Rev. Lett*. 99 (2007) 123603.

[8] Wang Z G, Ying P, Li P Y, *et al*. Switching suppression and enhancement of fluorescence and six-wave mixing by phase modulation [R]. *Scientific Reports* 3 (2013) 3417.

[9] Zhang Y Q, Wu Z K, Zheng H B, *et al*. Controllable nonreciprocity of six-wave mixing by a moving electromagnetically induced grating [J]. *Laser Phys*. 24 (2014) 045402.

[10] Zhu C J, Xiao Y, Senin A A, *et al*. Ouantum beating in Rb at 18.3 THz(608 cm^{-1}) detected by parametric six-wave mixing and sum-frequency generation in LiIO3[J]. *Phys. Rev. A* 75 (2007) 053405.

[11] Boyd R W, Malcuit M S, Gauthier D J, *et al*. Competition between amplified spontaneous emission and the four-wave-mixing process[J], *Phys. Rev. A* 35 (1987): 1648 - 1658.

[12] Katharakis M, Merlemis N, Serafetinides A, *et al*. Four-wave mixing and parametric four-wave mixing near the 4P-4S transition of the potassium atom[J]. *J. Phys. B* 35 (2002): 4969 - 4980.

[13] Miles R, Harris S E. Optical third-harmonic generation in alkali metal vapors[J], *IEEE J. Quantum. Electron*. QE-**9** (1973): 470 - 484.